

# Initial River Test of a Monostatic RiverSonde Streamflow Measurement System

Calvin C. Teague, Donald E. Barrick, and Peter M. Lilleboe  
CODAR Ocean Sensors, Ltd.  
Los Altos, California 94024  
(408) 773-8240  
cal@alpha.stanford.edu, COSDon@aol.com, petel@codaros.com

Ralph T. Cheng  
U. S. Geological Survey  
Menlo Park, California 94025  
(650) 329-4500  
rtcheng@usgs.gov

**Abstract**—A field experiment was conducted on May 7–8, 2002 using a CODAR RiverSonde UHF radar system at Vernalis, California on the San Joaquin River. The monostatic radar configuration on one bank of the river, with the antennas looking both upriver and downriver, provided very high-quality data. Estimates of both along-river and cross-river surface current were generated using several models, including one based on normal-mode analysis. Along-river surface velocities ranged from about 0.6 m/s at the river banks to about 1.0 m/s near the middle of the river. Average cross-river surface velocities were 0.02 m/s or less.

## I. INTRODUCTION

A new RiverSonde streamflow UHF (350 MHz) radar system was tested on May 7 and 8, 2002 along the San Joaquin River at Vernalis, California. In contrast to the first bistatic RiverSonde tests [1], [2], a monostatic geometry was used for this experiment with the radar antenna placed on one bank of the river. A sketch of the geometry is shown in Fig. 1 and the field installation is shown in Fig. 2. The instrumentation included *in-situ* acoustic sensors visible on the water, the RiverSonde system with its antenna on the near bank, and a microwave radar system (not discussed here) utilizing two parabolic dish antennas above the shelter. The monostatic geometry with a wide viewing angle proved almost ideal, with the downstream motion of the water spreading the echoes widely in Doppler frequency and almost all energy at a particular frequency bin coming from a single direction.

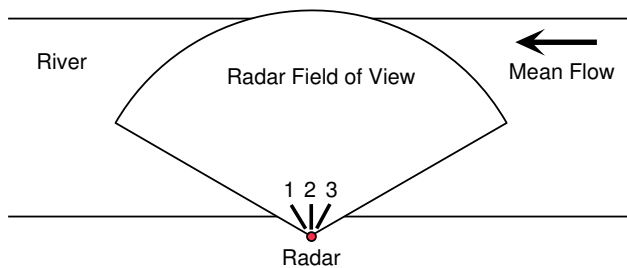


Fig. 1. Experiment geometry. The radar was on one bank of the river, with the mean water flow from right to left. The wide field of view of each antenna was across the river. The antennas are shown schematically; the 3 yagis were displaced along the river axis with a spacing of about 0.5 wavelength, and the two end yagis were rotated about 30° outward.



Fig. 2. Experimental setup at Vernalis, May, 2002. The RiverSonde antenna is on the near shore to the left of the building and receives signals from a wide angular sector, both upriver and downriver. Also visible are the narrow-beam microwave antennas above the building, and *in-situ* instrumentation in the water. Calibration of the RiverSonde antenna utilized a target carried by the cable across the river from the shelter to an anchor on the far bank.

Consequently, nearly all direction solutions were single-angle, which generally are more robust than dual-angle solutions.

Data were recorded for about an hour at each of several signal bandwidths; results using 5-m range resolution starting at 11:25 on May 8, 2002 are presented here. The hour-long run was divided into 20 segments of about 2.5 minutes each, with delay-Doppler and MUSIC direction finding [3] applied to each segment. Each segment yielded about 2500 radial current estimates spread from one bank to the other over about 140° in azimuth. Various processing techniques were applied to reduce the data, ranging from fitting to a uniform flow to modeling the flow as normal modes with constraints at the banks and boundaries of the analysis region, with the mode coefficients calculated from the data. Cross-channel velocity profiles were calculated for several along-channel positions, and the temporal behavior of these profiles was investigated. The radar-estimated flow ranged from about 0.6 to 1.0 m/s, depending on the location in the river channel, with differences in the details depending on the particular model used.



Fig. 3. Detail of the RiverSonde antennas. The middle antenna is used to illuminate a wide swath of water. Arrival directions of reflected signals are determined by processing signals received on all 3 yagis.

## II. EQUIPMENT

### A. Radar

The RiverSonde is derived from a standard SeaSonde system normally used at HF to observe currents on the ocean; it was retuned to a higher frequency consistent with the shorter water wavelengths expected in the river. At UHF the scattering is still predominantly Bragg [4], and approaching and receding wave energy can be separated and processed independently, except for a small portion of the spectrum near zero Doppler shift where the approaching and receding energy regions overlap. An interrupted chirp waveform with a bandwidth of 30 MHz was used, resulting in a range resolution of 5 m.

### B. Antenna

Considerable effort was put into the design of the antenna system. A four-element yagi was used for the transmit antenna, with a broad azimuthal pattern illuminating the water both upriver and downriver from the radar location. A 3-yagi array, consisting of the 4-element transmit yagi and two 5-element yagis displaced from the central transmitting yagi by about 0.5 m, was used for the receiver. Fig. 3 shows the antenna array. The yagis were designed using a real-valued genetic algorithm [5] to simultaneously optimize the directional response and feed-point impedance. Their performance was estimated using the computer program NEC2 [6] and verified by field calibration using a switched-dipole antenna as a transponder. Fig. 4 compares the phase of the NEC simulations with the field measurements; similar results (not shown) were observed for the amplitude response. The close agreement between the measurements and the NEC simulations indicates that the NEC results accurately represent the antenna performance. Fig. 4 displays the phases for zero depression angle, but the NEC predictions for the actual depression angle to the water surface (up to  $30^\circ$  at the near shore) were used in the MUSIC processing.

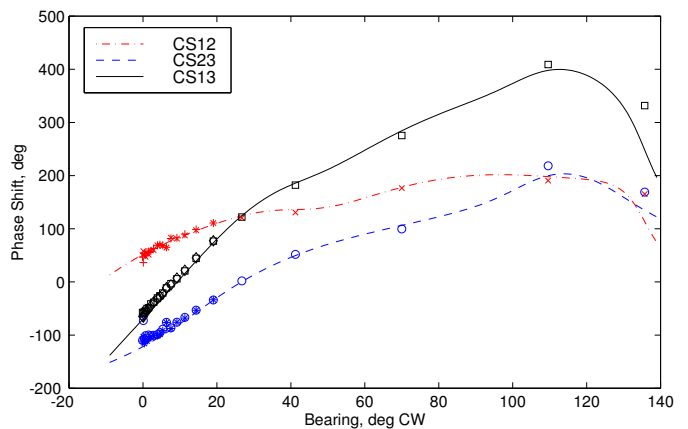


Fig. 4. Phase calibration at Vernalis. Lines are NEC predictions, points are measured values. The NEC predictions have been shifted vertically to account for cable delays in order to best match the measurements, but their shape is unchanged. CS12, CS23, CS13 refer to the phases of the cross-spectra between antennas 1&2, 2&3, and 1&3, respectively. Antennas are numbered as in Fig. 1. The transponder was carried on a cable stretched across the river, so measurements tend to cluster near broadside at the far bank.

## III. DATA PROCESSING

Conventional delay-Doppler processing was applied to the data. MUSIC direction finding [3] utilizing both the amplitude and phase responses of all 3 yagi antennas was used to locate the echoes. The direction-finding algorithm was applied independently at each frequency and delay bin, using an angular resolution of  $1^\circ$ . An example of the raw data (after median filtering to eliminate wild data points) is shown in Fig. 5; approximately 2800 radial current vectors are plotted. This figure represents just one segment of data, covering about 2.5 minutes, and 20 such segments covering about an hour were processed for this report.

### A. Uniform Current

The simplest current model is that of a uniform current, possibly with a small cross-river component. Assuming that model for the data of Fig. 5 results in an along-channel component of 0.975 m/s and a cross-channel component

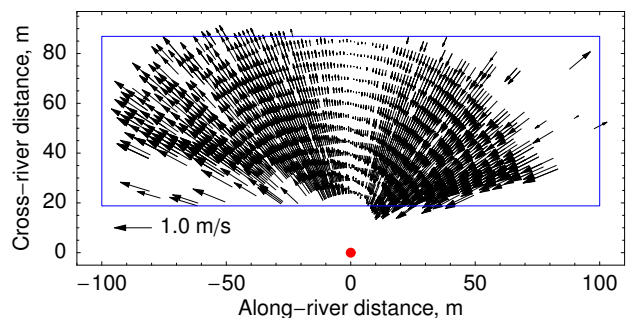


Fig. 5. Radial currents for one 2.5-minute data segment on May 8, 2002. Spurious vectors caused by personnel movement near the antennas have been removed using a median filter. The bounding box for the mode-fit calculations is shown by the inner rectangle, and the radar location is indicated by the dot at the origin.

of 0.021 m/s, with an RMS difference between the radial component of the model and the radial radar current velocity measurements of 0.069 m/s. Although a uniform model is useful in estimating the average flow, *in-situ* observations with acoustic sensors indicate significant cross-channel variation, and that variation is of considerable interest. Consequently, two other models were studied.

### B. Normal Modes Analysis

We considered a variation of a normal mode analysis (NMA) model [7] for river flow. In this model, the water is considered to be incompressible and the horizontal two-dimensional flow is expressed in terms of velocity potentials satisfying certain conditions at the boundaries. For the case of the river flow, we assumed a rectangular domain shown in Fig. 5 by the inner box. The boundary conditions were that normal flow at the banks is zero (certainly reasonable), and that the flow at the two ends of the rectangle is the same; that is, a “periodic boundary condition” in the along-river direction (perhaps not as reasonable but tractable). The ends of the rectangle are sufficiently far from the measurements so as to not influence results near the measurements, but near enough so that the periodic assumption is reasonable. This boundary condition avoids reflections at artificial boundaries at the open ends and the need for absorbing boundary conditions (which are complex). For the Vernalis experiment, the ends were placed  $\pm 100$  m from the radar location.

Eq. (5) of [8] or Eq. (1) of [7] represent an exact formulation for two-dimensional flow on any horizontal surface passing through the water, including the air-water interface that we are dealing with here. They are derived from the equation of 3-dimensional continuity for water, *i.e.*, the fact that it is incompressible. This horizontal flow can be expressed in terms of two, 2-dimensional scalar potentials. The horizontal surface velocity vector  $\vec{U} = [u, v]$  is thus given as

$$\vec{U} = \nabla \times [\hat{z}(-\Psi) + \nabla \times (\hat{z}\Phi)] \quad (1)$$

where  $\hat{z}$  is the vertical unit vector, approximately perpendicular to the mean water surface,  $\Psi$  is the stream function, and  $\Phi$  is the velocity potential. At a rigid boundary such as a river bank, the stream function satisfies the Dirichlet boundary condition and the velocity potential satisfies the Neumann boundary condition. Both of these conditions mean, in essence, that flow velocity normal to the bank boundary is zero, and there is no impedance to tangential flow along the bank, two perfectly reasonable assumptions.

The latter boundary conditions mean that the scalar potentials can be found from two second-order linear partial differential equations, Helmholtz equations, representing an eigenfunction expression for the 2-dimensional homogeneous solutions. For the stream function satisfying the Dirichlet condition at the bank,

$$\nabla^2 \psi_n + \nu_n \psi_n = 0, \quad \text{where } \psi_n|_{\Gamma} = 0 \quad (2a)$$

$$[u_n^D, v_n^D] = \left[ \frac{-\partial \psi_n}{\partial y}, \frac{\partial \psi_n}{\partial x} \right] \quad (2b)$$

where  $\psi_n$  is the  $n$ -th eigenfunction of the stream function  $\Psi$ ,  $\nu_n$  is the corresponding  $n$ -th eigenvalue and  $u_n^D$  and  $v_n^D$  are the velocity components in the  $x$  and  $y$  directions, respectively. For the velocity potential satisfying the Neumann condition at the bank,

$$\nabla^2 \phi_n + \mu_n \phi_n = 0, \quad \text{where } (\hat{\lambda} \cdot \nabla \phi_n)|_{\Gamma} = \frac{\partial \phi_n}{\partial \lambda}|_{\Gamma} = 0 \quad (3a)$$

$$[u_n^N, v_n^N] = \left[ \frac{\partial \phi_n}{\partial x}, \frac{\partial \phi_n}{\partial y} \right] \quad (3b)$$

where  $\phi_n$  is the  $n$ -th eigenfunction of the velocity potential  $\Phi$ ,  $\mu_n$  is the corresponding  $n$ -th eigenvalue and  $\hat{\lambda}$  is the direction perpendicular to the boundary.

In Eqs (2) and (3),  $\Gamma$  represents the boundary condition at the bank, where the normal flow is zero. The periodic boundary condition at the open ends is a departure from the analysis of [7]. The solutions to these eigensystems have eigenvalues  $\nu_n$  and  $\mu_n$ , while their eigenfunctions  $\psi_n$  and  $\phi_n$  are what we call the “normal modes.” In canonical coordinate systems like Cartesian and polar, these can be found in closed form as the trigonometric and Bessel functions. For general, arbitrary boundaries, these must be determined from finite-element numerical methods.

For a periodic boundary at  $x = \pm L/2$  and bank at  $y = \pm W/2$ , the velocity potential modes are

$$\phi_n(x, y) = \begin{cases} \cos(j2\pi x/L) \cos(m\pi y/W) & \text{for } j = 0, 1, 2, 3, \dots; m = 0, 2, 4, 6, \dots \\ \cos(j2\pi x/L) \sin(m\pi y/W) & \text{for } j = 0, 1, 2, 3, \dots; m = 1, 3, 5, 7, \dots \\ \sin(j2\pi x/L) \cos(m\pi y/W) & \text{for } j = 0, 1, 2, 3, \dots; m = 0, 2, 4, 6, \dots \\ \sin(j2\pi x/L) \sin(m\pi y/W) & \text{for } j = 0, 1, 2, 3, \dots; m = 1, 3, 5, 7, \dots \end{cases} \quad (4)$$

The corresponding stream modes are

$$\psi_n(x, y) = \begin{cases} \cos(j2\pi x/L) \cos(m\pi y/W) & \text{for } j = 0, 1, 2, 3, \dots; m = 1, 3, 5, 7, \dots \\ \cos(j2\pi x/L) \sin(m\pi y/W) & \text{for } j = 0, 1, 2, 3, \dots; m = 0, 2, 4, 6, \dots \\ \sin(j2\pi x/L) \cos(m\pi y/W) & \text{for } j = 0, 1, 2, 3, \dots; m = 1, 3, 5, 7, \dots \\ \sin(j2\pi x/L) \sin(m\pi y/W) & \text{for } j = 0, 1, 2, 3, \dots; m = 0, 2, 4, 6, \dots \end{cases} \quad (5)$$

Of course, the *velocity* modes to be fitted are the gradient and curl derivatives of these functions defined by Eqs. (3b) and (2b) earlier. In addition to the homogeneous modes of Eqs. (4) and (5), we included a constant velocity term to account for the mean current. The velocity model is the sum of a finite number of these gradient and curl derivatives, with unknown coefficients. For each location for where radar

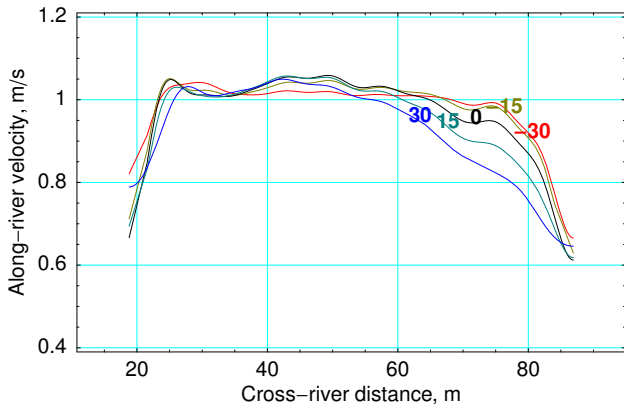


Fig. 6. Profiles of mean down-river velocity on May 8, 2002 at 5 locations along the river separated by 15 m. The origin is at the radar antenna. Numbers on each plot denote the along-river location (in meters) of the profile.

measurements are available, the model is evaluated in terms of the unknown coefficients, and the radial component of the model is equated to the radial radar measurement. Repeating this step over all available radar measurements results in an overdetermined set of equations for the coefficients. The coefficients are determined by a least-squares solution to this set of equations.

We allowed modes up to 20th order in the direction across the river (values of  $m$  above) for the along-river velocity component. We found that the solution was unstable for high-order modes along the river (that is, values of  $j$  above) for both the along-river and cross-river velocity component, so we limited values of  $j$  to 2. With these constraints, stable solutions were found for both the along-river and cross-river velocities. The mean along-river velocity profile over 20 segments of data covering an hour is shown in Fig. 6. Five profiles running across the river at the location of the radar and  $\pm 15$  m and  $\pm 30$  m upriver (positive) and downriver (negative) from the radar are displayed. The velocity is about 1.0 m/s in the middle of the channel and falls off to about 0.6 m/s at the banks. There is some variation of the profile with position upriver from the radar, and less so at downriver positions. This may be due to the effects of a bend in the river about 250 m upriver from the radar; the channel was straight downriver from the radar. The cross-channel velocity was 0.02 m/s or less.

### C. Direct Fit

A third model assumes a current with significant variation across the river, but none in the along-river direction, for both the along-river and cross-river velocity components. The data from several directions symmetrically offset from the broadside direction are combined, and the  $u$  (along-river) and  $v$  (cross-river) velocity components are directly calculated from

$$r_1 = v \cos \theta + u \sin \theta \quad (6a)$$

$$r_2 = v \cos \theta - u \sin \theta \quad (6b)$$

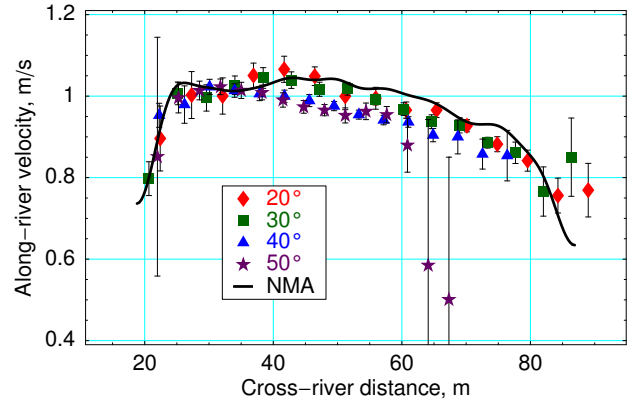


Fig. 7. Direct solution for along-river velocity for each data segment, obtained at angles of  $\pm 20^\circ$ ,  $30^\circ$ ,  $40^\circ$  and  $50^\circ$  from broadside. Current is assumed to vary only in the cross-river direction. The mean fit obtained from the normal modes model is shown for comparison by the solid line.

where  $r_1$  is the radial velocity (positive away from the radar) measured in a direction  $\theta$  clockwise from the broadside direction, and  $r_2$  is the corresponding radial component measured in a direction  $\theta$  counterclockwise from the broadside direction. The solution to the above equations is

$$u = \frac{r_1 - r_2}{2 \sin \theta} \quad (7a)$$

$$v = \frac{r_1 + r_2}{2 \cos \theta} \quad (7b)$$

The procedure outlined above was applied to each of the 20 segments of data, for directions  $\theta$  of  $\pm 20^\circ$ ,  $30^\circ$ ,  $40^\circ$  and  $50^\circ$  from the broadside direction, averaging the radials within  $5^\circ$  of each direction. The results for the along-channel current  $-u$  are shown in Fig. 7. The symbols denote the average current for those directions for which at least 3 segments of data yielded solutions, and the error bars show the sample standard deviation over the available data. The solid curve is the mean of the normal modes fit of Fig. 6 for comparison; it is not a fit to the points of Fig. 7. The direct solution appears to give a slightly lower estimate than the normal modes procedure, with a higher standard deviation for larger angles from broadside. For large angles off broadside, the distance between the measurements for the clockwise and counterclockwise directions is greater, and the assumption that these two directions see the same current is not as good as for smaller angles off broadside. The mean cross-channel velocity  $v$  was between 0 and 0.07 m/s across the channel.

## IV. COMPARISON WITH IN-SITU MEASUREMENTS

In addition to the UHF and microwave radar measurements, extensive *in-situ* measurements were made by USGS personnel using two acoustic instruments [9]. An acoustic Doppler current profiler (ADCP) and a "BoogieDopp" (BD) were used together at 20–25 stations across the river, and at each station detailed vertical velocity profiles were collected. The performance of the ADCP is limited by the relatively shallow

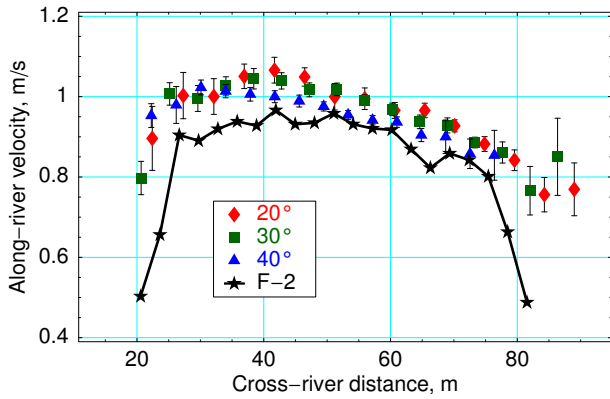


Fig. 8. Direct solution RiverSonde data, for directions  $\theta$  of  $\pm 20^\circ$ ,  $30^\circ$  and  $40^\circ$  from the broadside direction, as in Fig. 7 (symbols), and BoogieDopp (BD) data (solid line) from the F-2 beam [9]. The origin of the distance scale for the BD data (the river bank) is displaced 16 m from the location of the RiverSonde antenna.

water at Vernalis, so the data from the BD are compared with the radar data. The topmost BD measurement is about 0.11 m below the water surface. Fig. 8 compares the direct-solution RiverSonde data starting at 11:25 and the BD data from the F-2 beam starting at 13:14 on May 8, 2002. The shape of the profile is in good agreement between the two sensors, with the RiverSonde velocities about 10% higher than the BD velocities.

## V. DISCUSSION

All of the data processing techniques for the UHF radar data gave similar results, with the “direct solution” giving slightly lower velocity estimates than the others. All of the radar estimates are higher than the *in-situ* acoustic measurements, particularly near the radar, and in somewhat better agreement in the middle of the channel. The source of the difference is not yet clear, but it should be noted that the effective depth of the radar is quite shallow. If the depth scales similarly to the observations at HF which indicated an effective depth of about 8% of the water wavelength [10], in agreement with theoretical predictions [11], then the effective depth of the radar measurement is only about 0.04 m, and the acoustic measurement reflects a current at about three times that depth. There may be current shear in the topmost layers, most likely generated by wind effects. The phase velocity of the 0.45 m Bragg waves is 0.84 m/s, and winds were sufficient to generate those waves. In analogy with the results we have seen at HF in which we saw significant vertical shear in the presence of winds of the order of the phase velocity of the waves [10], the winds present during this experiment may have generated some vertical shear in the topmost few centimeters of the water.

## VI. SUMMARY

The monostatic geometry employed in this experiment worked very well. Strong returns were obtained with about 1 W of power out to nearly 100 m. Looking across the mean flow resulted in a broad Doppler spectrum which provided predominantly single-angle direction solutions. Each segment of data yielded about 2500 radial vectors, so the solutions even for 20 modes were stable. The radar velocities were somewhat higher than the *in-situ* acoustic measurements, and the source of that difference is still under investigation, but the overall results are quite encouraging. Additional long-term measurements at the same site are planned for the near future.

## ACKNOWLEDGMENT

The authors would like to acknowledge the members of the USGS Hydro-21 Committee who supported the field work at Vernalis, California.

## REFERENCES

- [1] C. C. Teague, D. E. Barrick, P. Lilleboe, and R. T. Cheng, “Canal and river tests of a RiverSonde streamflow measurement system,” in *IEEE 2001 International Geoscience and Remote Sensing Symposium Proceedings*, New York, July 2001, IEEE, pp. 1288–1290, IGARSS’01, Sydney, Australia.
- [2] D. E. Barrick, C. C. Teague, P. M. Lilleboe, R. T. Cheng, and J. W. Gartner, “Profiling river surface velocities and volume flow estimation with bistatic UHF RiverSonde radar,” in *IEEE Seventh Working Conference on Current Measurement Technology Proceedings*, New York, March 2003, IEEE, This volume.
- [3] R. O. Schmidt, “Multiple emitter location and signal parameter estimation,” *IEEE Trans. on Antennas and Propagation*, vol. AP-34, pp. 276–280, 1986.
- [4] D. E. Barrick, “Theory of HF/VHF propagation across the rough sea. Part II: Application to HF/VHF propagation above the sea,” *Radio Science*, vol. 6, pp. 527–533, 1971.
- [5] “Yagi genetic optimizer, ver. 3,” DOS program YGO3. Available through <http://www.qsl.net/wb6tpu/swindex.html>.
- [6] G. J. Burke and A. J. Poggio, “Numerical electromagnetics code (NEC)—method of moments,” Tech. Rep. TD116, Lawrence Livermore Laboratory, 1981.
- [7] B. L. Lipphardt Jr., A. D. Kirwan Jr., C.E. Grosch, J. K. Lewis, and J. D. Paduan, “Blending HF radar and model velocities in Monterey Bay through normal mode analysis,” *J. Geophys. Res.*, vol. 105, pp. 3425–3450, February 2000.
- [8] V. N. Eremeev, L. M. Ivanov, and A. D. Kirwan Jr., “Reconstruction of oceanic flow characteristics from quasi-Lagrangian data 1. Approach and mathematical methods,” *J. Geophys. Res.*, vol. 97, pp. 9733–9741, June 1992.
- [9] R. T. Cheng and J. W. Gartner, “Complete velocity distribution in river cross-sections measured by acoustic instruments,” in *IEEE Seventh Working Conference on Current Measurement Technology Proceedings*, New York, March 2003, IEEE, This volume.
- [10] C. C. Teague, J. F. Vesecky, and Z. R. Hallock, “A comparison of multifrequency HF radar and ADCP measurements of near-surface currents during COPE-3,” *IEEE Journal of Oceanic Engineering*, vol. 26, no. 3, pp. 399–405, July 2001.
- [11] R. H. Stewart and J. W. Joy, “HF radio measurement of surface currents,” *Deep-Sea Research*, vol. 21, pp. 1039–1049, 1974.